Structure of the UHRF1 Tandem Tudor Domain Bound to a Methylated Non-histone Protein, LIG1, Reveals Rules for Binding and Regulation

Satomi Kori, Laure L. Ferry, Tomohiro Jimenji, Shohei Matano, Rumie Matsumura, Takashi Oda, Noriyuki Kodera, Pierre-Antoine Defossez, Kyohei Arita

Structure of the UHRF1 Tandem Tudor Domain Bound to a Methylated Non-histone Protein, LIG1, Reveals Rules for Binding and Regulation

Possible alternative titles:

Structural basis for recognition of a methylated non-histone protein by the UHRF1 tandem tudor domain

Structure of the UHRF1 Tandem Tudor Domain bound to a methylated non-histone protein, LIG1, reveals rules for binding and regulation.

Satomi Kori[1], Laure Ferry[2], Tomohiro Jimenji[1], Shohei Matano[1] Rumie Matsumura[1], Takashi Oda[1], Noriyuki Kodera[3,4,5], Pierre-Antoine Defossez[2]§ and Kyohei Arita[1,5]§

1: Yokohama City University, Department of Medical Life Sciences, Yokohama 230-0045, Japan.
2: Univ. Paris Diderot, Sorbonne Paris Cité, Epigenetics and Cell Fate, UMR 7216 CNRS, 75013 Paris, France.
3: Department of Physics, Kanazawa University, Kakuma-machi, Kanazawa, 920-1192, Japan.
4: Bio-AFM Frontier Research Center, Kanazawa University, Kanazawa, 920-1192, Japan.
5: JST, PRESTO, 4-1-8 Honcho, Kawaguchi, Saitama, 332-0012, Japan.

#: These authors contributed equally to this work
§: Corresponding authors: pierre-antoine.defossez@univ-paris-diderot.fr ; aritak@yokohama-cu.ac.jp

ABSTRACT (200 words)

DNA methylation is essential in mammalian cells, and its patterns are faithfully reproduced at each round of DNA replication. The protein UHRF1 is crucial for this process: it binds recently replicated regions and causes the recruitment of the DNA methyltransferase DNMT1, ensuring maintenance methylation. The Tandem Tudor Domain (TTD) of UHRF1 is critical for its function; it binds H3K9me2/3, but also unmethylated linker regions within UHRF1 itself, causing auto-inhibition. Recently, it was reported that a methylated histone-like region of DNA Ligase 1 (LIG1K126me3) outcompetes H3K9me2/3 for TTD binding, permitting UHRF1 recruitment to chromatin. Here we report the crystal structure of the UHRF1 TTD bound to a methylated LIG1 peptide. The structure is validated by functional cellular assays and reveals the key residues for interaction and the mechanism for high affinity binding of LIG1. Furthermore, single molecule analysis demonstrates that binding of LIG1 changes the overall structure of UHRF1 to a flexible conformation, suggesting that UHRF1 auto-inhibition is relieved. This is the first reported structure of UHRF1 bound to a methylated non-histone protein, and our results provide structural insight into how UHRF1 performs its key function in epigenetic maintenance.

INTRODUCTION

DNA methylation and histone modifications are major epigenetic marks that regulate diverse cellular events by modulating the structure and function of chromatin (1, 2). In mammals, DNA methylation occurs mostly at the 5th position of cytosine in CpG dinucleotides and plays key roles in development, X-chromosome inactivation, genome imprinting and carcinogenesis (3–6). In proliferating cells, the pattern of DNA methylation has to be re-established after each cycle of DNA replication, and two proteins are known to be key in this process, as their absence causes a similar phenotype of progressive DNA demethylation (7–11). The first protein involved is the maintenance DNA methyltransferase, DNMT1, and the other is the protein UHRF1 (Ubiquitin-like, containing PHD and RING finger domains, 1).

UHRF1 contains five annotated domains: Ubiquitin-Like (UBL); Tandem Tudor Domain (TTD); Plant Homeo Domain (PHD); SET and RING Associated (SRA), and Really Interesting New Gene (RING), and their associated linkers. The SRA is essential for function and specifically recognizes hemi-methylated DNA, which is generated after DNA replication (12–14). Subsequently the RING domain, which has E3 ubiquitin ligase activity, ubiquitylates K14, K18 and/or K23 on histone H3 (hereafter H3), which allows DNMT1 recruitment onto recently replicated sites, (15–17). The PHD and TTD work cooperatively to recognize the heterochromatin mark H3K9me2/3: the PHD recognizes the N-terminus of the histone, while the TTD accommodates the methylated H3K9me2/3 residue in an aromatic cage (18–21). In addition, the TTD also interacts with unmethylated lysine and arginine-rich linkers within UHRF1 itself: the "spacer" which follows the SRA domain (spacer^{UHRF1}) and the "linker 2" between TTD

and PHD finger ($L2^{UHRF1}$) (18, 21–23). These intramolecular interactions lead to a "closed" overall structure and the auto-inhibition of DNA binding and E3 activities (22–24).

We recently showed that the TTD interacts with a histone-like sequence within a replication protein, DNA Ligase 1 (LIG1) (25). Molecularly, LIG1 contains an intrinsically disordered region (IDR) at its N-terminus (residues 1-200), within which residues 118-130 are similar to the H3 N-terminal tail (residues 1-12), and LIG1K126 is in a sequence environment similar to H3K9. Furthermore, LIG1K126 is methylated by the lysine methyltransferases G9a and GLP (EHMT1 and EHMT2) *in vitro* and in cells. We found that a LIG1K126me3 peptide largely outcompetes H3K9me2/3 peptides for binding to the UHRF1 TTD. We also reported that the aromatic cage of the TTD was necessary for binding, yet a number of molecular questions remain open as to how UHRF1 interacts with this methylated non-histone protein. What are the similarities between H3K9me2/3 and LIG1K126me3 binding? What are the differences, and how do they contribute to the higher affinity binding to LIG1? What is the effect of LIG1 binding to the overall UHRF1 architecture and function?

To address these questions, we have solved the crystal structure of the UHRF1 TTD in complex with a methylated LIG1 peptide. The structure, complemented by mutagenesis and functional assays reveals key residues for the interaction, sheds light on the mechanism for high affinity binding of LIG1 to TTD, and indicates that the binding event causes a large-scale molecular reorganization within UHRF1. Our data provide the first insight into UHRF1 binding to a methylated non-histone protein, and contribute to understanding its key role in epigenetic maintenance.

MATERIAL AND METHODS

Peptide preparation

The human LIG1 peptides, residues 118-130 (NH^2-^{118}IPKRRTARKQLPK^{130}-COOH) harboring K126me3, R121A-K126me3, R125A-K126me3 or T123ph-K126me3, and histone H3 K9me3 (NH^2-^{1}ARTKQTAR-K(me3)-STGGKAPRKQ^{19}-COOH) were purchased from Toray Research Center (Tokyo, Japan).

Crystallography of TTD and its complex with LIG1-K126me3 peptide

The TTD of human UHRF1 (residues 123-285) was expressed as a fusion protein with glutathione S-transferase (GST) and small ubiquitin like modifier-1 (SUMO-1) at its N-terminus. Cell culture and purification were performed according to our previous report (18). Cocrystallization of this wild-type TTD with the LIG1-K126me3 peptide was unsuccessful, so we used instead a mutant version of the TTD, deleting residues 167-175. The protocols of cell culture and purification of the deletion mutant are the same as for wild-type TTD.

Crystals of apo-TTD were obtained by using a reservoir solution containing 0.1 M Bis-Tris (pH 6.5), 200 mM ammonium acetate and 25% (w/v) polyethylene glycol (PEG) 3,350 at 4°C. The crystals were cryoprotected by 20% (v/v) ethylene glycol. Diffraction data were collected at a wavelength of 1.5418 Å on a RIGAKU R-AXIS IV^{++} equipped with MicroMax 007 (RIGAKU). Data were processed with program XDS package (26) and Aimless (27) at 1.7 Å resolution. The structure of apo-TTD was solved by molecular replacement method using the coordinates of the human UHRF1 TTD (PDB; 3DB3) as a search model. Molecular replacement and model refinement were performed using PHASER (28) and PHENIX (29). After several cycles of refinement, the model converged well at 1.7 Å resolution with a crystallographic *R*-factor of 17.9 % and free *R*-factor of 24.2%.

The TTD: LIG1-K126me3 complex was prepared by adding a 1.5-molar excess of the LIG1-K126me3 peptide to the protein before concentration using an Amicon concentrator with a 10,000 Da cutoff (Millipore). The crystal was obtained using a 30 mg/ml concentration of the complex at 20°C and the hanging drop vapor diffusion method with a reservoir solution containing 100 mM Tris-HCl (pH 7.0), 200 mM tri-potassium phosphate and 20% (w/v) PEG3350. The crystal was directly frozen in liquid nitrogen using a cryoprotectant containing 20% (v/v) ethylene glycol. The X-ray diffraction data were collected at a wavelength of 0.98000 Å on a Pilatus3 6M detector

in beam line BL-17A at Photon Factory (Tsukuba, Japan) and scaled at 2.65 Å resolution with the program XDS package and Aimless. After molecular replacement by PHASER and several cycle of model refinement by PHENIX, $2|F_o|$ - $|F_c|$ difference Fourier map corresponding to LIG1-K126me3 were unambiguously observed. The final model converged at 2.65 Å resolution with a crystallographic *R*-factor of 23.1% and a free *R*-factor of 28.8%.

The crystallographic data and refinement statistics are given in Table 1. The figures were generated using Pymol (http://www.pymol.org).

ITC measurements

Cell culture and purification of UHRF1 PHD were performed according to our previous report (18). Mutants of TTD (residues 123-285) were generated by the Quickchange mutagenesis method (Agilent Technologies). Purified UHRF1 TTD or its mutants were buffer-exchanged using Superdex 200 Increase 10/300 GL (GE HealthcareScience) equilibrated with the ITC buffer (10 mM HEPES-NaOH (pH 7.5), 150 mM NaCl, 0.25 mM tris(2-carboxyethyl)phosphine Hydrochloride (TCEP)). Lyophilized LIG1 peptides (residues 118-130) and H3K9me3 peptide (residues 1-19) were dissolved in the same buffer. A MicroCal LLC calorimeter, VP-ITC (MicroCal), was used for the ITC measurements. The TTD solution in the calorimetric cell was titrated with the peptide solution at 293 K. The data were analyzed with the software ORIGIN (MicroCal) using a one-site model.

Fluorescent three-hybrid assay (F3H)

The starting plasmids for F3H were: full-length human UHRF1 cloned in pEGFP-C2 (plasmid PAD1543) (25) and full-length human LIG1, cloned in pmRFP-C2 (plasmid PAD1766) (25). The various mutations were introduced by Gibson Assembly Cloning. The F3H assay were performed as previously described (30), using BHK cells. Each experiment was carried out at least twice independently, with 100 cells scored in blind in each repetition.

SAXS

Protein preparation of the TTD-PHD, residues 123-366, is described in a previous paper (18). The TTD-PHD in complex with LIG1-K126me3 or H3K9me3 was prepared by adding a 2.0-molar excess of the peptide to the protein. Before SAXS measurements, the proteins were loaded to Superdex 200 Increase 10/300GL to eliminate aggregates. SAXS measurements were performed at 4 °C with a

MicroMax007HF X-ray generator (Rigaku) equipped with a PILATUS100K detector (DECTRIS) at a distance of 561 mm from the sample. Circular averaging of the scattering intensities was carried out to obtain one-dimensional scattering data $I(q)$ as a function of q ($q = 4\pi\sin\theta/\lambda$, where 2θ is the scattering angle and λ is the X-ray wavelength 1.5418 Å). To correct for interparticle interference, $I(q)$ data were collected at three different protein concentrations (1.0, 1.5, and 2.0 mg/ml in 20 mM Tris-HCl (pH 7.5), 150 mM NaCl, 5 mM DTT, 5 mM β-mercaptoethanol, 2 mM TCEP and 10 μM ZnOAc). The total exposure times were 3 hours for each sample. Because the intensity profile did not indicate a concentration effect, the correction for interparticle interference was not applied. To estimate the molecular weight of samples, $I(q)$ data were collected for chicken egg white lysozyme (4.9 mg/ml in 20 mM Tris-HCl (pH 7.5), 150 mM NaCl). The data were processed by using the software applications embedded in the ATSAS package (31). The radius of gyration R_g and forward scattering intensity $I(0)$ were estimated from the Guinier plot of $I(q)$ in the smaller angle region of $qR_g < 1.3$. The distance distribution function $P(r)$ was calculated in the program GNOM (32), where the experimental $I(q)$ data were used in a q-range from 0.031 to 0.300 Å^{-1}. The maximum particle dimension D_{max} was estimated from the $P(r)$ function as the distance r for which $P(r) = 0$. The molecular weight of the sample was estimated by comparing $I(0)/c$ (where c is the protein concentration) of the sample to that of lysozyme.

HS-AFM observations

To produce the full-length protein with N-terminal 6×histidine (His6) tag, the full-length human UHRF1 cDNA was sub-cloned into pGEX6P-1 (GE HealthcareScience). Bacterial culture and purification of the protein was performed according to our previous report (16).

HS-AFM imaging was performed in solution at room temperature using a laboratory-built HS-AFM setup (33, 34) as described previously (35). In brief, a glass sample stage (diameter, 2 mm; height, 2 mm) with a thin mica disc (1 mm in diameter and ~0.05 mm thick) glued to the top by epoxy was attached onto the top of a Z-scanner by a drop of nail polish. A freshly cleaved mica surface was prepared by removing the top layers of mica using Scotch tape. Then, a drop (2 μl) of diluted protein sample (ca. 3 nM) in dilution buffer (20 mM Tris-HCl (pH 7.5), 500 mM NaCl and 10% glycerol) was placed on the mica surface. After incubation for 3 min at room temperature, the mica surface was rinsed with 20 μl of the observation buffer (20 mM Tris-HCl (pH 7.5), 150 mM NaCl) to remove floating samples. The sample stage was then immersed in a liquid cell containing ~60 μl of the observation buffer. AFM Imaging was carried out in the

tapping mode, using small cantilevers (BLAC10DS-A2, Olympus, Tokyo, Japan); resonant frequency, ~0.5 MHz in water; quality factor, ~2 in water; spring constant, ~0.1 N/m. The cantilever's free oscillation amplitude A_0 and set-point amplitude A_s were set at 1−2 nm and ~0.9 × A_0, respectively. The imaging rate, scan size and the pixel size for each AFM image are 150 ms/frame, 60 × 60 nm^2 and 80 × 80 pixels, respectively.

Analysis of AFM images

For analysis, AFM images were pretreated with a low-pass filter to remove spike noise and with a flatten filter to make the overall xy-plane flat, using a laboratory built software as described before (35). This software is available at https://elifesciences.org/content/4/e04806/article-data-fig-data-supplementary-material. The heights of molecules were measured semi-automatically using the following steps. First, the most probable highest point near the highest point of the molecule was selected manually. Second, the actual highest point was automatically determined by searching a 10 × 10 pixel area (typically 7.5 × 7.5 nm^2) around the selected point.

2D correlation coefficients were calculated between the HS-AFM images of the first frame and each of the frames within the Region of Interest (ROI) (*i.e.,* the first frame is the reference). The sizes of the ROIs were about 25×25 nm^2. The 2D correlation coefficient was calculated frame-by-frame for each ROI. The 2D correlation coefficient r is defined as,

$$r = \frac{\sum_m \sum_n (H_{mn} - \overline{H})(R_{mn} - \overline{R})}{\sqrt{(\sum_m \sum_n (H_{mn} - \overline{H})^2 (\sum_m \sum_n (R_{mn} - \overline{R})^2}}$$

in which H_{mn} and R_{mn} are the heights at the pixel point (m, n) in the ROI to be analyzed and the reference ROI of the reference frame, respectively. $\overline{H}$ and $\overline{R}$ are the mean values of the height matrices H and R, respectively.

RESULTS

The TTD in complex with LIG1-K126me3 peptide adopts a canonical structure

Cocrystallization of the wild-type human TTD (residues 123-285) with the LIG1K126me3 peptide was not successful. After optimization trials, we used for co-crystallization a variant TTD (vTTD from here on), with deletion of a flexible loop (residues 167-175). This deletion mutant has essentially the same binding properties for LIG1-K126me3 as the wild type TTD (data not shown). The LIG1 peptide contained residues 118-130 of the human protein, with the key lysine K126 trimethylated (K126me3).

We determined the crystal structure of vTTD with LIG1-K126me3 peptide at 2.65 Å resolution (Table 1); in the crystal, an asymmetric unit contained two TTD:LIG1-K126me3 complexes. The structures of the two TTD in the unit were identical (root mean square deviation (RMSD) of Cα atoms 1.401 Å over the 125 Cα atoms) (Supplementary Figure S1A). The structure of LIG1-K126me3 peptides in the asymmetric unit was also identical (RMSD of Cα atoms 0.456 Å) (Supplementary Figure S1B). The twelve successive residues from Ile118 to Pro129 showed clear electron density in a |*F*o| - |*F*c| omit map (Figure 1A, B), and are described hereafter. Finally, for comparison purposes, we also determined the structure of unliganded TTD; the resolution obtained was 1.70 Å (Table 1).

The overall TTD structure was virtually identical with or without the LIG1-K126me3 peptide (RMSD of Cα atoms 0.8~1.6 Å) (Supplementary Figure S1A), implying that binding of the LIG1-K126me3 did not lead to the structural rearrangement of the TTD. As in previously published structures (23, 36), the 1st and 2nd tudor domains comprised a five-stranded β-barrel fold, and the two domains were separated

by a groove (TTD groove from here on, Supplementary Figure S1A). The LIG1-K126me3 peptide interacted in an extended conformation with TTD groove and, within the peptide, residues Arg121 to Lys126me3 contacted TTD residues (Figure 1A and E).

Two regions of the LIG1-K126me3 peptide establish dense contacts with the TTD

The structure showed that two clusters of dense contacts between TTD and LIG1 peptide participated to the stable complex formation. First, the aromatic cage comprising Phe152, Tyr188 and Tyr191 of UHRF1 interacted with tri-methyl moiety of K126me3 in LIG1 (Figures 1C and E). Second, the side chain of LIG1Arg121 was inserted into the hole of the TTD groove; there, the guanidino group and aliphatic portion of Arg121 were recognized by multiple hydrogen bonds and hydrophobic interactions with side chains of UHRF1Asp142 and Met224, Trp238 and Phe278, respectively (Figures 1D and E). Of these positions, Asp142, Met224 and Trp238 are almost invariant within UHRF1 homologs found in animal species, whereas Phe278 is conserved but at a lower level (Supplementary Figure S2. NB: we should swap figures S2 and S3, as we use the alignment first in the text). In addition to these dense contacts, the side chains of Arg122 and Arg125 of LIG1 were recognized by the side chain of Glu276 and the main chain of Asp190 of TTD, respectively (Figures 1C-E). Glu193 of TTD also supported the binding to LIG1Arg125 by long-range electrostatic interaction (~3.7 Å) (Figure 1C). The side chain of LIG1Thr123 formed additional hydrogen bonds with the side chain of UHRF1Trp238 (Figure 1D). Finally, the main chains of Arg121, Arg122, Ala124 and K126me3 in LIG1 were also involved in the interaction with TTD (Figure 1E).

Our published work (25), as well as data presented here, suggest that the TTD of UHRF1 has much higher affinity for methylated LIG1 than for its other reported interactors: H3K9me3, spacer^{UHRF1} and L2^{UHRF1} (18, 22, 23, 36). To understand the basis for this preference, we compared the peptide sequences and structural data for all these interactions; as a reference point in the alignments we assign position "N" to LIG1Arg121 (Figure 2A). The sequences of the interacting peptides show similarities, such as basic residues preferred at positions N-1, N, and N+1, Ser or Thr at N+2, and small aliphatic residues at N+3. The structural data, showed large differences in the extent to which the residues interact with the TTD (Figure 2A-E). LIG1 had the highest number of interactions, as the side chains of residues N, N+1, N+2, N+4 and N+5 interacted with the TTD. In contrast, H3K9me3 interaction with the TTD did not engage N+1 nor N+4. When bound to the TTD, the spacer^{UHRF1} and L2^{UHRF1} failed to engage either N+1, N+4 or N+5 residues, although the N-1 position of spacer^{UHRF1} formed hydrophilic interaction with the TTD that were not seen with the other peptides. Collectively, it is likely that the larger number of hydrophilic and hydrophobic interactions formed between LIG1-K126me3 and TTD underlie the higher binding affinity.

Mutational analysis validates the structural data and uncovers a phospho-switch regulation

To validate our structural data and quantify the contribution of individual residues to the interaction, we performed isothermal titration calorimetry (ITC) experiments using WT or mutated versions of the TTD and LIG1 peptide (Figure 3A; Supplementary Figure S2). The values obtained with WT partners were consistent with

our previous reports (18, 25): the TTD bound LIG1-K126me3 with a K_D = 9.11 ± 3.80 nM and LIG1-K126me0 with a K_D = 250 ± 38 nM (Figure 3A). In contrast to the binding of H3K9me3, no detectable interaction was observed between LIG1-K126me3 and UHRF1 PHD finger, indicating that binding to LIG1 is limited to the TTD groove (Supplementary Figure S2).

We tested several mutations of the TTD (Figure 3A; Supplementary Figure S3). The mutation with the most deleterious effect was D142A, which obliterated any detectable binding. The second most deleterious change was inactivation of the aromatic cage, using the double mutation Y188A/Y191A which resulted in detectable but vastly reduced affinity for LIG1K126me3 (K_D = 5.38 ± 0.49 μM). Mutation W238A also had a large effect, reducing the affinity a hundred-fold (K_D = 1.06 ± 0.04 μM). Finally, mutations E193A and E276A had smaller but measurable effects on the UHRF1/LIG1-K126me3 interaction. All of these critical residues are shared between UHRF1 and UHRF2, so we tested the possibility that UHRF2 might also bind LIG1; ITC experiments showed that it was indeed the case (Supplementary Figure S3).

Next, we introduced mutations in the LIG1-K126me3 peptide. The R121A change had a severe effect, reducing binding at least 6000-fold (Figure 3A, K_D > 55 μM); in contrast the R125A mutation only led to a slight binding reduction (K_D =21.4 ± 1.1 nM). Finally, it has been observed that phosphorylation of the N+2 position inhibits the interaction of TTD with H3K9me3 (20), $L2^{UHRF1}$ (18) and $spacer^{UHRF1}$ (22, 23), so we tested whether this might also occur in the case of LIG1. We synthetized a peptide in which LIG1K126 was trimethylated, and LIG1T123 phosphorylated; this peptide interacted extremely poorly with the TTD (K_D > 104 μM, Figure 3A), establishing that phosphorylation at N+2 is indeed inhibitory to the interaction.

We also examined the interaction by an independent technique, the fluorescent three-hybrid assay (F3H) (30). In this approach, proteins bearing fluorescent tags are co-expressed in an engineered mammalian cell line, which is designed so that the GFP-tagged protein will be recruited to a nuclear focus. The percentage of cells in which the RFP-tagged protein forms a focus colocalizing with the GFP focus is then recorded, and provides a direct estimate of the interaction propensity in cells (Schematic in Figure 3B). We carried out this assay with full-length UHRF1 fused to GFP, and full-length LIG1 fused to DsRed, using WT proteins or introducing the mutations studied by ITC. The F3H results agreed very well with ITC: mutation D142A in UHRF1 had a severe effect, W238A was less marked, and E193A and/or E276A had smaller effects (Figure 3C; Supplementary Figure S4A). Within LIG1, the R121A mutation totally abrogated interaction, and so did the phosphomimetic T123D mutation. A striking difference with the ITC results is that the LIG1R125A mutation led to total loss of interaction in the F3H assay (Figure 3D; Supplementary Figure S4B). A likely explanation is that the LIG1R125A mutant protein fails to be methylated on K126, as G9a requires an RK motif in its target to catalyze lysine methylation (37).

Altogether, the data from ITC and F3H are fully consistent with the structure we obtained. Moreover, they reveal that the ionic interaction between Asp142 of TTD and Arg121 of LIG1 plays a foremost role in the binding, followed by the hydrophobic interaction between LIG1K126me3 and the TTD hydrophobic cage. Lastly, we have shown that the interaction can be negatively regulated by phosphorylation of LIG1T123.

Binding to LIG1 changes the arrangement of the TTD-PHD module and the overall UHRF1 structure

In the TTD-PHD functional module, $L2^{UHRF1}$ interacts with the TTD groove and positions the PHD relative to the TTD (18, 22, 23). H3K9me3 binding does not change the overall arrangement of the TTD-PHD, as judged by crystal structure and small angle X-ray scattering (SAXS) (18, 38). In contrast, mutating key residues of $L2^{UHRF1}$ (R295 and R296) or employing a compound that binds the groove, 4-benzylpiperidine-1-carboximidamide (BPC), does make the TTD-PHD less compact (18, 38). We asked if this would also be observed upon LIG1 binding and for this we used SAXS (Figures 4A; Supplementary Figures S5A-C).

We used the distance distribution function $P(r)$ to calculate the radius of qyration (R_g) and D_{max} value (Figure 4A; Supplementary Figure S5B and C). The numbers obtained for apo-TTD-PHD were similar to those previously reported (18, 38), and they were not affected by the addition of H3K9me3 (Figure 4A), again agreeing with our previous report. In contrast, the addition of LIG1K126me3 caused a marked increase in the radius of gyration, implying a rearrangement of the TTD-PHD module to a more open form. The structural change is similar to TTD-PHD R295A/R296A mutation, which lost the interaction between $L2^{UHRF1}$ and the TTD groove, thus suggesting that LIG1-K126me3 binding extruded the $L2^{UHRF1}$ from the groove.

To reveal the effect of LIG1-K126me3 binding to the overall UHRF1 structure, we switched to a different approach: single-molecule analysis of the full length UHRF1 by High-Speed Atomic Force Microscopy (HS-AFM), a powerful technique for real-space and real-time observations of macromolecules (39). Imaging of the N-terminal histidine-tagged UHRF1 on Ni^{2+} coated mica demonstrated that apo-UHRF1 appeared as a compact molecule with a diameter of 3.89 ± 0.28 nm estimated from height analyses (Figure 4B and C; Supplementary Movie 1 and Figure S6). In contrast, binding

of LIG1-K126me3 significantly decreased the compactness of the particle: its height was diminished to 2.44 ± 0.25 nm (Figure 4B and C; Supplementary Movie 2 and Figure S7), indicating that the structure of UHRF1 was changed to a more open form. HS-AFM also yielded information about the dynamics of the molecules: the correlation coefficients for sequential HS-AFM images of apo-UHRF1 were distributed around 0.867 ~ 0.969, indicating a rather static structure, whereas those of UHRF1:LIG1 complexes were lower (0.404 ~ 0.915), indicative of increased conformational flexibility (Figure 4D; Supplementary Figure S6 and S7).

DISCUSSION

We report the first structure of the UHRF1 TTD bound to a methylated non-histone protein, LIG1. This interaction is physiologically important, as it permits the recruitment of UHRF1 to replicating DNA, and the maintenance of DNA methylation, an essential epigenetic mark in mammals (25). Our structural data are validated by independent biochemical and cellular approaches, and they shed light on 3 important questions: what distinguishes LIG1 interaction from interaction with other TTD binders, what may regulate this interaction, and how the interaction allosterically regulates UHRF1.

Structure of the UHRF1 TTD complexed with LIG1 reveals commonalities and differences with other interactors

A first conclusion from our data is that the TTD engages LIG1 in a manner similar to its other targets: the LIG1 peptide was extended in the TTD groove as previously reported for H3, the $L2^{UHRF1}$ and $spacer^{UHRF1}$. Another commonality between the various interactions is that they all involve a basic residue (Arg or Lys, R121 in the case of LIG1) in the binder, which penetrates deep in the groove and forms an electrostatic interaction with Asp142 of UHRF1, a residue that is highly conserved through evolution (Supplementary Figure S3). Finally, another similarity with previous structures is that the methylated lysine (LIG1K126me3) is accommodated by the aromatic cage formed of UHRF1 Phe152, Tyr188, and Tyr 191, as is the case for H3K9me3 (18, 21, 36).

These similarities imply that the binding of the TTD to its various interactors must be mutually exclusive, raising the question of how LIG1 can outcompete the other

binders. Indeed $L2^{UHRF1}$ and $spacer^{UHRF1}$ form with the TTD intramolecular interactions, which should have a much higher probability of contact, especially at lower UHRF1 concentrations. As for H3K9me3 molecules, they form intermolecular interactions with the TTD, but they outnumber LIG1 by a factor of ~100 (25). To be able to engage the TTD, it is expected that LIG1 should have an affinity significantly higher than the other binders, and this is in fact what we observe (25). In the crystal structure, Arg122 and Arg125 of LIG1 formed interactions not seen for H3K9me3, $spacer^{UHRF1}$ or $L2^{UHRF1}$. Based on these and other observations, we suggest that the high avidity of LIG1 for the TTD results from a combination of several hydrophilic and hydrophobic interactions that are not formed by the other binders.

Another piece of insight gained from the structure is that the UHRF1 residues that interact with LIG1 are conserved in UHRF2, and we experimentally validated that the UHRF2 TTD interacts with LIG1. Therefore LIG1 binding is probably a shared activity, and the fact that UHRF1 and UHRF2 are not exchangeable (PMID:21598301; 22064703) must involve one or several other functions.

Possible modes of regulation

The interaction between LIG1 and UHRF1 is highly affine *in vitro*, and easily detectable in cells. Nevertheless, it seems likely that the complex undergoes dissociation at some points in time and space, so that LIG1 can fulfill its catalytic activity —the ligation of Okazaki fragments— while UHRF1 remains on replicated DNA to ensure H3 ubiquitylation, DNMT1 recruitment, and possibly allosteric DNMT1 activation (15–17, 40, 41). How may the interaction between LIG1 and UHRF1 be dissociated?

A first and obvious possibility is the demethylation of LIG1K126me3, which

reduces affinity ~30-fold *in vitro*. Of note, ~80% of LIG1 molecules carry K126 methylation in cells (25), suggesting that if K126 demethylation occurs, it is a transient event. Future work may reveal if such an event exists, and which enzyme is involved.

Our data reveal at least 3 additional possibilities. The first is methylation of LIG1R121, which is predicted to disrupt the key electrostatic interactions with UHRF1D142. The second is methylation of LIG1R125, which is predicted to prevent G9a from methylating LIG1K126, and should therefore phenocopy our LIG1R125A mutation. FEN1, the flap endonuclease acting just before LIG1 during replication, is regulated by arginine methylation (42), and it could be of interest in the future to ask whether LIG1 is also targeted on R121 and R125 by arginine methyltransferases. Finally, the third is phosphorylation of LIG1Thr123; we experimentally showed that it decreases affinity for the TTD ~10000-fold. Interestingly, this mechanism could be conserved between interactions, as phosphorylation of the equivalent residues (H3Thr6, Ser298 in $L2^{UHRF1}$, and Ser651 in $spacer^{UHRF1}$) has a similar effect (18, 23, 43). Thr123 of LIG1 is within a consensus sequence for Protein Kinase Cβ (PKCβ) (44), and this kinase phosphorylates H3Thr6 (45), so it could also possibly regulate the LIG1/UHRF1 interaction.

LIG1 as an allosteric effector of UHRF1: functional consequences

Several reports have unambiguously established that full-length UHRF1 undergoes intramolecular interactions, causing it to present a compact physical aspect, causing the inhibition of its molecular activities (22–24). Using HS-AFM, we confirm that UHRF1 is compact, and further observe that its conformation becomes more open and more dynamic once it interacts with LIG1. Therefore, LIG1 can be added to

phosphatidylinositol 5-phosphate, hemimethylated DNA, and H3K9me3 as an allosteric regulator of UHRF1.

In spite of this similarity, LIG1 also presents a key difference with H3K9me3 with respect to its effect on the TTD and PHD domains. Indeed it has been shown by several investigators that these two domains form a functional module, in which the PHD is precisely positioned relative to the TTD thanks to $L2^{UHRF1}$, which binds the TTD groove. The addition of H3K9me3 does not disrupt this architecture: instead H3K9me3 adopts a constrained conformation so that its N terminus binds the PHD, and its C terminus binds the TTD (18, 20). In clear contrast, our SAXS experiments show that LIG1 does modify the TTD-PHD module, towards a more open conformation; presumably this happens by displacing $L2^{UHRF1}$ from the groove. Our ITC experiments also show that the PHD does not detectably bind the LIG1 peptide, and this is consistent with expectations as LIG1 does not present the free N-terminal $^{1}ARTK^{4}$ motif that is critical for interaction with the PHD (18, 19, 46, 47). Therefore, our data suggest that, when UHRF1 is bound to LIG1, the PHD domain is released and free to engage in other intra- or inter-molecular interactions. These complex dynamics may be necessary to order, in space and time, the different functions that UHRF1 has to fulfill: recruitment to recently replicated DNA, methylation of histones, and activation of DNMT1.

Taken together, our results contribute to a better understanding of the critical epigenetic regulator UHRF1, and will guide future experiments to further study its functions.

ACCESSION NUMBER

The crystal structures of the apo-TTD and its complex with LIG1-K126me3 peptide have been deposited in the Protein Data Bank under accession code YYYY and XXXX, respectively.

SUPPLEMENTARY DATA

ACKNOWLEDGEMENTS

We would like to thank the beamline staff at the Photon Factory for X-ray data collection.

FUNDING

This study was supported by a PRESTO from JST (K.A.). PAD was supported by Association pour la Recherche contre le Cancer (ARC2014), and by Agence Nationale de la Recherche (ANR-15-CE12-0012-01 and ANR-11-LABX-0071 under ANR-11-IDEX-0005-01).

Conflict of interest statement: None declared.

FIGURE LEGENDS

Figure 1. Structure of the UHRF1 TTD in complex with a LIG1-K126me3 peptide. (A) Overall structure of TTD:LIG1-K126me3 complex. 1st and 2nd tudor domains are shown as yellow-green and pale-green surface models, respectively. LIG1 is depicted as magenta stick model. (B) The LIG1 and $|F_o|$ - $|F_c|$ omit map contoured at 2 σ are colored magenta and blue, respectively. (C), Recognition of R125-K126me3 and (D), R121-A124 of LIG1 by the TTD. Color schemes are the same as in Figure 1A. Water molecules are represented as black balls. (E), Schematic diagram of LIG1-K126me3 recognition by the TTD. The LIG1 backbone and side chains are shown in black and TTD residues in green. Dotted lines and black arcs with spokes indicate hydrogen bonds and hydrophobic interactions respectively.

Figure 2. Structural comparison of TTD binding partners.

(A), Sequence alignment of LIG1, H3, spacer^{UHRF1} and L2^{UHRF1}. Arg121 of LIG1 is defined as position 'N'. Residues from N to N+5 are colored pink, green yellow, cyan, orange and magenta, respectively. The residues underlined have a side chain that interacts with the TTD. Structure around the TTD groove in complex with (B) LIG1-K126me3, (C) H3K9me3 (PDB ID: 2L3R), (D) spacer^{UHRF1} (PDB ID: 5IAY) and (E) L2 ^{UHRF1} (PDB ID: 3ASK). Each peptide is shown as stick model and the color schemes are same in Figure 2A. Red and blue on the surface of TTD indicate hydrophilic and hydrophobic interaction residues, respectively.

Figure 3. Mutation analysis confirms the structural data and uncovers a negative regulation by phosphorylation.

(A), Determination of binding affinities by ITC. TTD with the indicated mutations and LIG1 with the indicated the PTMs were subjected to ITC experiments and the derived K_D values are expressed as the fold-decrease from that of interaction between wt TTD and LIG1-K126me3. K_D values with standard deviations determined by ITC are also depicted under the bar in the graph. (B), Principle of the F3H assay. (C), Mutations in the UHRF1 TTD affect interaction with LIG1. (D), Mutations in LIG1 affect interaction with the UHRF1 TTD.

Figure 4. Decreased compactness and increased dynamics of UHRF1 upon LIG1 binding.

(A), SAXS experiments on the TTD-PHD module. $P(r)$ functions are shown for 1.5 mg/ml of apo-TTD-PHD (blue) and its complex with H3K9me3 (green) and LIG1-K126me3 peptides (red). R_g and D_{max} values are also shown. (B), Successive HS-AFM images showing representative molecular shape of apo-UHRF1 (upper) and its complex with LIG1-K126me3 (lower). Frame rate, 150 ms/frame; scan area, 60 × 60 nm^2 with 80 × 80 pixels; Z-scale, 4.5 nm in apo-UHRF1 and 3.5 nm in the complex. (C) Height distributions: blue bars for the apo-UHRF1; pink bars for the UHRF1:LIG1-K126me3 complex. Blue and red lines indicate single-Gaussian fitting for apo-UHRF1 and UHRF1:LIG1-K126me3 complex, respectively. (D) Time courses of correlation coefficients between the sequential HS-AFM images of apo-UHRF1 (blue) and its complex with LIG1-K126me3 (red).

REFERENCES

1. Bird,A.P. and Wolffe,A.P. (1999) Methylation-induced repression--belts, braces, and chromatin. *Cell*, **99**, 451–4.
2. Probst,A. V., Dunleavy,E. and Almouzni,G. (2009) Epigenetic inheritance during the cell cycle. *Nature Reviews Molecular Cell Biology*, **10**, 192–206.
3. Ballabio,A. and Willard,H.F. (1992) Mammalian X-chromosome inactivation and the XIST gene. *Current opinion in genetics & development*, **2**, 439–47.
4. Costello,J.F., Frühwald,M.C., Smiraglia,D.J., Rush,L.J., Robertson,G.P., Gao,X., Wright,F.A., Feramisco,J.D., Peltomäki,P., Lang,J.C., *et al.* (2000) Aberrant CpG-island methylation has non-random and tumour-type-specific patterns. *Nature genetics*, **24**, 132–8.
5. Smith,Z.D. and Meissner,A. (2013) DNA methylation: roles in mammalian development. *Nature Reviews Genetics*, **14**, 204–220.
6. Schübeler,D. (2015) Function and information content of DNA methylation. *Nature*, **517**, 321–6.
7. Bostick,M., Kim,J.K., Esteve,P.-O., Clark,A., Pradhan,S. and Jacobsen,S.E. (2007) UHRF1 Plays a Role in Maintaining DNA Methylation in Mammalian Cells. *Science*, **317**, 1760–1764.
8. Sharif,J., Muto,M., Takebayashi,S., Suetake,I., Iwamatsu,A., Endo,T.A., Shinga,J., Mizutani-Koseki,Y., Toyoda,T., Okamura,K., *et al.* (2007) The SRA protein Np95 mediates epigenetic inheritance by recruiting Dnmt1 to methylated DNA. *Nature*, **450**, 908–912.
9. Strahl,B.D. and Allis,C.D. (2000) The language of covalent histone modifications.

Nature, **403**, 41–45.

10. Smets,M., Link,S., Wolf,P., Schneider,K., Solis,V., Ryan,J., Meilinger,D., Qin,W. and Leonhardt,H. (2017) DNMT1 mutations found in HSANIE patients affect interaction with UHRF1 and neuronal differentiation. *Human Molecular Genetics*, **26**, 1522–1534.
11. von Meyenn,F., Iurlaro,M., Habibi,E., Liu,N.Q., Salehzadeh-Yazdi,A., Santos,F., Petrini,E., Milagre,I., Yu,M., Xie,Z., *et al.* (2016) Impairment of DNA Methylation Maintenance Is the Main Cause of Global Demethylation in Naive Embryonic Stem Cells. *Molecular Cell*, **62**, 848–861.
12. Arita,K., Ariyoshi,M., Tochio,H., Nakamura,Y. and Shirakawa,M. (2008) Recognition of hemi-methylated DNA by the SRA protein UHRF1 by a base-flipping mechanism. *Nature*, **455**, 818–821.
13. Avvakumov,G. V, Walker,J.R., Xue,S., Li,Y., Duan,S., Bronner,C., Arrowsmith,C.H. and Dhe-Paganon,S. (2008) Structural basis for recognition of hemi-methylated DNA by the SRA domain of human UHRF1. *Nature*, **455**, 822–825.
14. Hashimoto,H., Horton,J.R., Zhang,X., Bostick,M., Jacobsen,S.E. and Cheng,X. (2008) The SRA domain of UHRF1 flips 5-methylcytosine out of the DNA helix. *Nature*, **455**, 826–829.
15. Qin,W., Wolf,P., Liu,N., Link,S., Smets,M., Mastra,F. La, Forné,I., Pichler,G., Hörl,D., Fellinger,K., *et al.* (2015) DNA methylation requires a DNMT1 ubiquitin interacting motif (UIM) and histone ubiquitination. *Cell Research*, **25**, 911–929.
16. Nishiyama,A., Yamaguchi,L., Sharif,J., Johmura,Y., Kawamura,T., Nakanishi,K., Shimamura,S., Arita,K., Kodama,T., Ishikawa,F., *et al.* (2013) Uhrf1-dependent

H3K23 ubiquitylation couples maintenance DNA methylation and replication. *Nature*, **502**, 249–253.

17. Ishiyama,S., Nishiyama,A., Saeki,Y., Moritsugu,K., Morimoto,D., Yamaguchi,L., Arai,N., Matsumura,R., Kawakami,T., Mishima,Y., *et al.* (2017) Structure of the Dnmt1 Reader Module Complexed with a Unique Two-Mono-Ubiquitin Mark on Histone H3 Reveals the Basis for DNA Methylation Maintenance. *Molecular Cell*, **68**, 350–360.e7.
18. Arita,K., Isogai,S., Oda,T., Unoki,M., Sugita,K., Sekiyama,N., Kuwata,K., Hamamoto,R., Tochio,H., Sato,M., *et al.* (2012) Recognition of modification status on a histone H3 tail by linked histone reader modules of the epigenetic regulator UHRF1. *Proceedings of the National Academy of Sciences*, **109**, 12950–12955.
19. Rajakumara,E., Wang,Z., Ma,H., Hu,L., Chen,H., Lin,Y., Guo,R., Wu,F., Li,H., Lan,F., *et al.* (2011) PHD finger recognition of unmodified histone H3R2 links UHRF1 to regulation of euchromatic gene expression. *Molecular cell*, **43**, 275–284.
20. Rothbart,S.B., Dickson,B.M., Ong,M.S., Krajewski,K., Houliston,S., Kireev,D.B., Arrowsmith,C.H. and Strahl,B.D. (2013) Multivalent histone engagement by the linked tandem Tudor and PHD domains of UHRF1 is required for the epigenetic inheritance of DNA methylation. *Genes & development*, **27**, 1288–98.
21. Cheng,J., Yang,Y., Fang,J., Xiao,J., Zhu,T., Chen,F., Wang,P., Li,Z., Yang,H. and Xu,Y. (2013) Structural insight into coordinated recognition of trimethylated histone H3 lysine 9 (H3K9me3) by the plant homeodomain (PHD) and tandem tudor domain (TTD) of UHRF1 (ubiquitin-like, containing PHD and RING finger domains, 1) protein. *The Journal of biological chemistry*, **288**, 1329–39.

22. Gelato,K.A., Tauber,M., Ong,M.S., Winter,S., Hiragami-Hamada,K., Sindlinger,J., Lemak,A., Bultsma,Y., Houliston,S., Schwarzer,D., *et al.* (2014) Accessibility of different histone H3-binding domains of UHRF1 is allosterically regulated by phosphatidylinositol 5-phosphate. *Molecular cell*, **54**, 905–19.

23. Fang,J., Cheng,J., Wang,J., Zhang,Q., Liu,M., Gong,R., Wang,P., Zhang,X., Feng,Y., Lan,W., *et al.* (2016) Hemi-methylated DNA opens a closed conformation of UHRF1 to facilitate its histone recognition. *Nature communications*, **7**, 11197.

24. Harrison,J.S., Cornett,E.M., Goldfarb,D., DaRosa,P.A., Li,Z.M., Yan,F., Dickson,B.M., Guo,A.H., Cantu,D. V, Kaustov,L., *et al.* (2016) Hemi-methylated DNA regulates DNA methylation inheritance through allosteric activation of H3 ubiquitylation by UHRF1. *eLife*, **5**.

25. Ferry,L., Fournier,A., Tsusaka,T., Adelmant,G., Shimazu,T., Matano,S., Kirsh,O., Amouroux,R., Dohmae,N., Suzuki,T., *et al.* (2017) Methylation of DNA Ligase 1 by G9a/GLP Recruits UHRF1 to Replicating DNA and Regulates DNA Methylation. *Molecular Cell*, **67**, 550–565.e5.

26. Kabsch,W. (2010) XDS. *Acta crystallographica. Section D, Biological crystallography*, **66**, 125–32.

27. Evans,P.R. and Murshudov,G.N. (2013) How good are my data and what is the resolution? *Acta crystallographica. Section D, Biological crystallography*, **69**, 1204–14.

28. McCoy,A.J., Grosse-Kunstleve,R.W., Adams,P.D., Winn,M.D., Storoni,L.C. and Read,R.J. (2007) Phaser crystallographic software. *Journal of applied crystallography*, **40**, 658–674.

29. Afonine,P. V, Grosse-Kunstleve,R.W., Echols,N., Headd,J.J., Moriarty,N.W.,

Mustyakimov,M., Terwilliger,T.C., Urzhumtsev,A., Zwart,P.H. and Adams,P.D. (2012) Towards automated crystallographic structure refinement with phenix.refine. *Acta crystallographica. Section D, Biological crystallography*, **68**, 352–67.

30. Herce,H.D., Deng,W., Helma,J., Leonhardt,H. and Cardoso,M.C. (2013) Visualization and targeted disruption of protein interactions in living cells. *Nature Communications*, **4**, 2660.

31. Petoukhov,M. V., Franke,D., Shkumatov,A. V., Tria,G., Kikhney,A.G., Gajda,M., Gorba,C., Mertens,H.D.T., Konarev,P. V. and Svergun,D.I. (2012) New developments in the *ATSAS* program package for small-angle scattering data analysis. *Journal of Applied Crystallography*, **45**, 342–350.

32. Svergun,D.I. and IUCr (1992) Determination of the regularization parameter in indirect-transform methods using perceptual criteria. *Journal of Applied Crystallography*, **25**, 495–503.

33. Ando,T., Uchihashi,T., Kodera,N., Yamamoto,D., Miyagi,A., Taniguchi,M. and Yamashita,H. (2008) High-speed AFM and nano-visualization of biomolecular processes. *Pflugers Archiv : European journal of physiology*, **456**, 211–25.

34. Ando,T., Kodera,N., Takai,E., Maruyama,D., Saito,K. and Toda,A. (2001) A high-speed atomic force microscope for studying biological macromolecules. *Proceedings of the National Academy of Sciences of the United States of America*, **98**, 12468–72.

35. Uchihashi,T., Kodera,N. and Ando,T. (2012) Guide to video recording of structure dynamics and dynamic processes of proteins by high-speed atomic force microscopy. *Nature Protocols*, **7**, 1193–1206.

36. Nady,N., Lemak,A., Walker,J.R., Avvakumov,G. V., Kareta,M.S., Achour,M.,

Xue,S., Duan,S., Allali-Hassani,A., Zuo,X., *et al.* (2011) Recognition of Multivalent Histone States Associated with Heterochromatin by UHRF1 Protein. *Journal of Biological Chemistry*, **286**, 24300–24311.

37. Rathert,P., Dhayalan,A., Murakami,M., Zhang,X., Tamas,R., Jurkowska,R., Komatsu,Y., Shinkai,Y., Cheng,X. and Jeltsch,A. (2008) Protein lysine methyltransferase G9a acts on non-histone targets. *Nature chemical biology*, **4**, 344–6.

38. Houliston,R.S., Lemak,A., Iqbal,A., Ivanochko,D., Duan,S., Kaustov,L., Ong,M.S., Fan,L., Senisterra,G., Brown,P.J., *et al.* (2017) Conformational dynamics of the TTD-PHD histone reader module of UHRF1 reveals multiple histone binding states, allosteric regulation and druggability. *Journal of Biological Chemistry*, 10.1074/jbc.M117.799700.

39. Ando,T., Uchihashi,T. and Scheuring,S. (2014) Filming Biomolecular Processes by High-Speed Atomic Force Microscopy. *Chemical Reviews*, **114**, 3120–3188.

40. Bashtrykov,P., Jankevicius,G., Jurkowska,R.Z., Ragozin,S. and Jeltsch,A. (2014) The UHRF1 Protein Stimulates the Activity and Specificity of the Maintenance DNA Methyltransferase DNMT1 by an Allosteric Mechanism. *Journal of Biological Chemistry*, **289**, 4106–4115.

41. Berkyurek,A.C., Suetake,I., Arita,K., Takeshita,K., Nakagawa,A., Shirakawa,M. and Tajima,S. (2014) The DNA Methyltransferase Dnmt1 Directly Interacts with the SET and RING Finger-associated (SRA) Domain of the Multifunctional Protein Uhrf1 to Facilitate Accession of the Catalytic Center to Hemi-methylated DNA. *Journal of Biological Chemistry*, **289**, 379–386.

42. Guo,Z., Zheng,L., Xu,H., Dai,H., Zhou,M., Pascua,M.R., Chen,Q.M. and Shen,B.

(2010) Methylation of FEN1 suppresses nearby phosphorylation and facilitates PCNA binding. *Nature chemical biology*, **6**, 766–73.

43. Rothbart,S.B., Krajewski,K., Nady,N., Tempel,W., Xue,S., Badeaux,A.I., Barsyte-Lovejoy,D., Martinez,J.Y., Bedford,M.T., Fuchs,S.M., *et al.* (2012) Association of UHRF1 with methylated H3K9 directs the maintenance of DNA methylation. *Nature Structural & Molecular Biology*, **19**, 1155–1160.

44. Wang,Y., Zhang,W., Jin,Y., Johansen,J., Johansen,K.M., Eisen,A., Koonin,E.V., Fouts,D.L., Wrightsman,R., Manning,J.E., *et al.* (2001) The JIL-1 tandem kinase mediates histone H3 phosphorylation and is required for maintenance of chromatin structure in Drosophila. *Cell*, **105**, 433–43.

45. Metzger,E., Imhof,A., Patel,D., Kahl,P., Hoffmeyer,K., Friedrichs,N., Müller,J.M., Greschik,H., Kirfel,J., Ji,S., *et al.* (2010) Phosphorylation of histone H3T6 by PKCbeta(I) controls demethylation at histone H3K4. *Nature*, **464**, 792–6.

46. Hu,L., Li,Z., Wang,P., Lin,Y. and Xu,Y. (2011) Crystal structure of PHD domain of UHRF1 and insights into recognition of unmodified histone H3 arginine residue 2. *Cell research*, **21**, 1374–8.

47. Lallous,N., Legrand,P., McEwen,A.G., Ramón-Maiques,S., Samama,J.-P. and Birck,C. (2011) The PHD finger of human UHRF1 reveals a new subgroup of unmethylated histone H3 tail readers. *PloS one*, **6**, e27599.

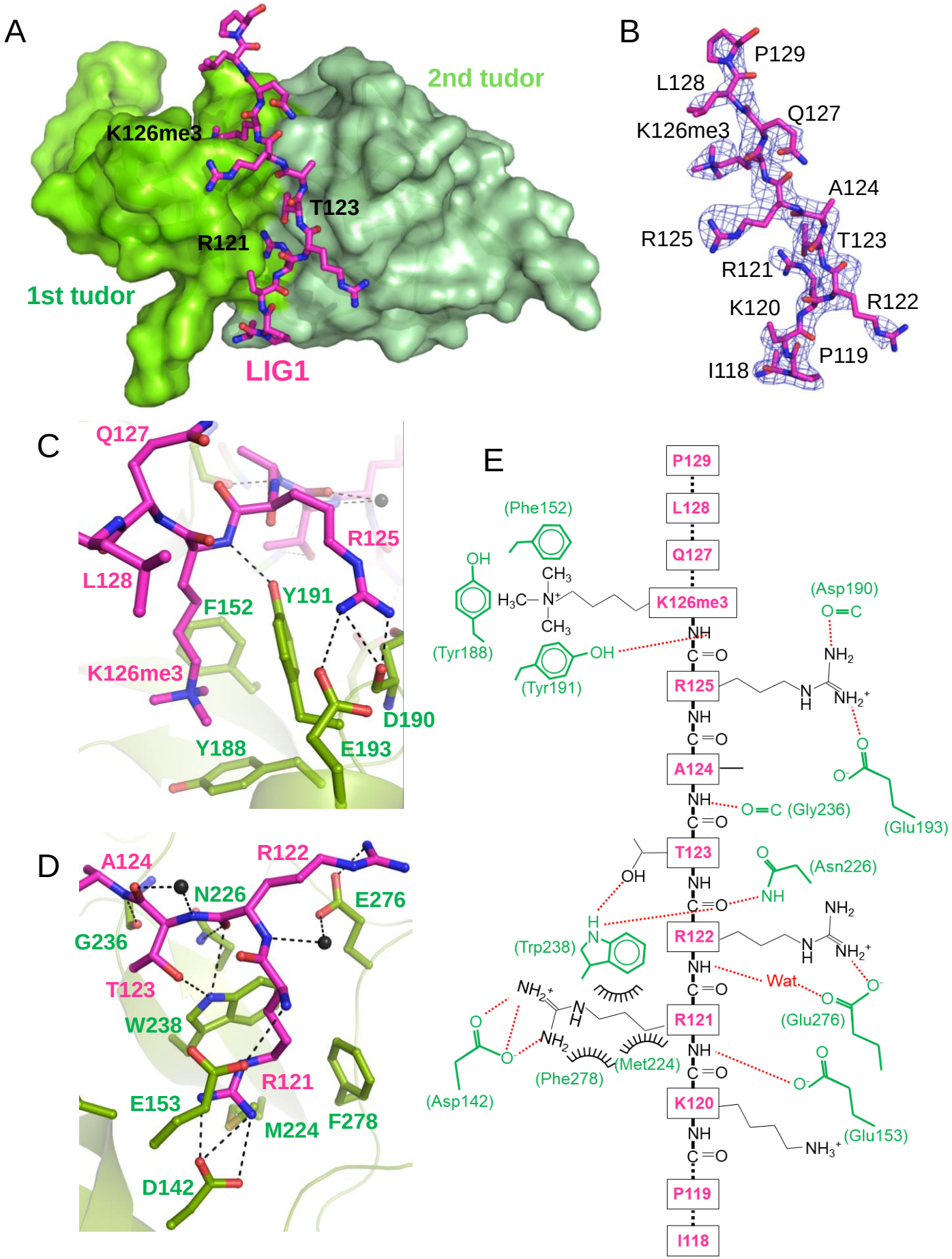
A
2nd tudor
K126me3
T123
R121
1st tudor
LIG1
B
P129
L128
Q127
K126me3
A124
R125
T123
R121
K120
R122
P119
I118
C
Q127
L128
R125
F152
Y191
K126me3
D190
Y188
E193
D
A124
R122
N226
E276
G236
T123
W238
R121
E153
M224
F278
D142
E
P129
L128
Q127
K126me3
R125
A124
T123
R122
R121
K120
P119
I118
(Phe152)
(Tyr188)
(Tyr191)
(Asp190)
(Gly236)
(Glu193)
(Asn226)
(Trp238)
Wat
(Glu276)
(Asp142)
(Phe278)
(Met224)
(Glu153)

Figure 1

A

				N-1	N	N+1	N+2	N+3	N+4	N+5			
LIG1 (118-129)	I	P	K	R	R	T	A	R	Kme3	Q	L	P
H3 (1-11)	A	R	T	K	Q	T	A	R	Kme3	S	T	
spacer^{UHRF1} (645-657)	G	K	W	K	R	K	S	A	G	G	G	P	S
L2^{UHRF1} (292-301)	N	P	M	R	R	K	S	G	P	S			

B

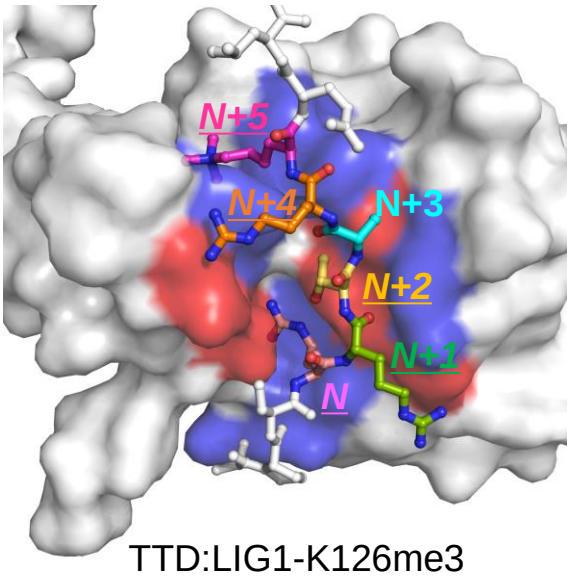

TTD:LIG1-K126me3

C

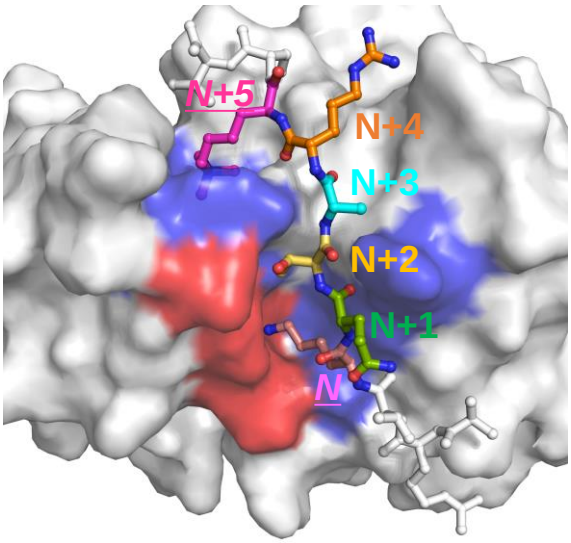

TTD:H3K9me3

D

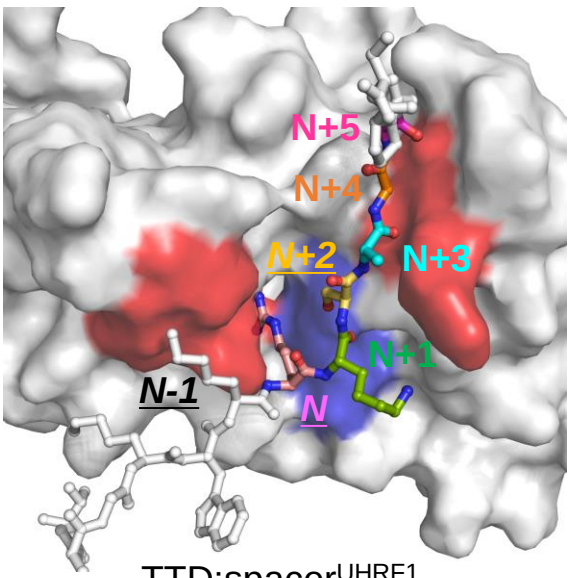

TTD:spacer^{UHRF1}

E

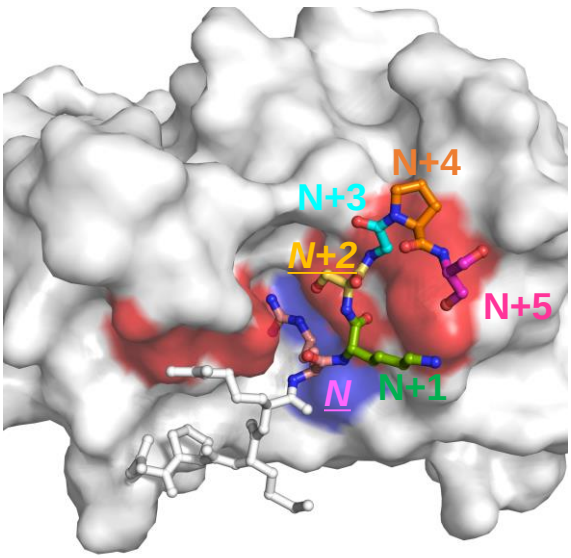

TTD:L2^{UHRF1}

Figure 2

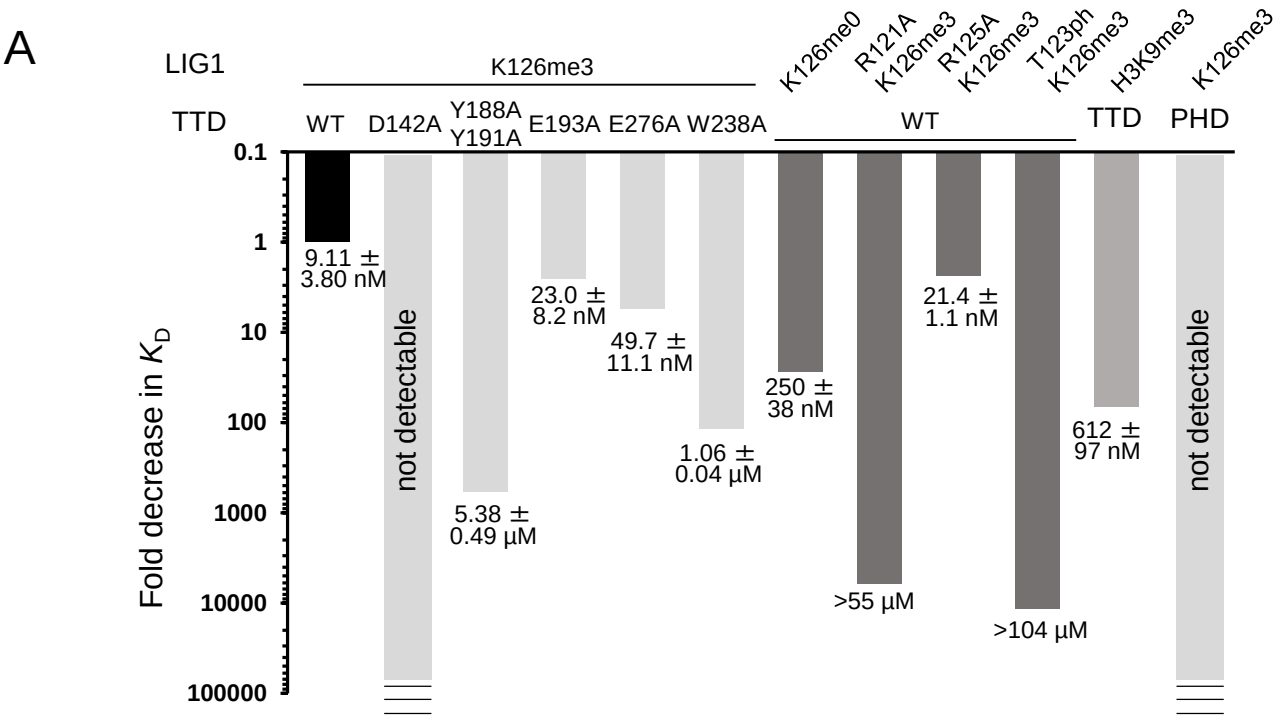

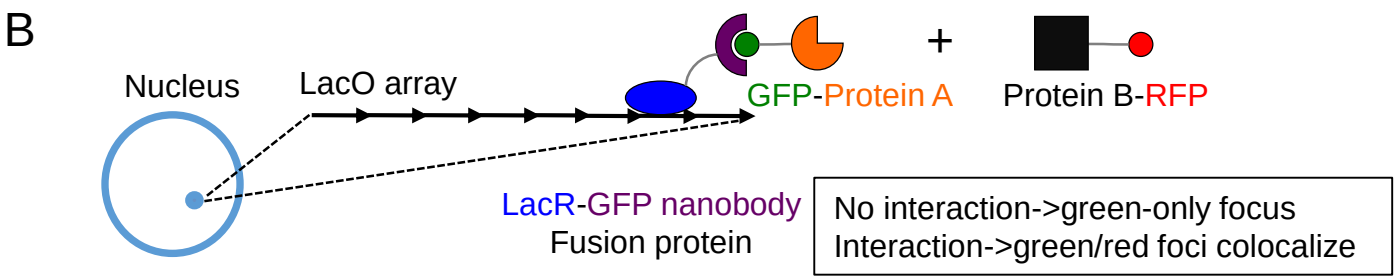

C

Plasmid cotransfected with DsRed-LIG1: GFP-UHRF1 with following mutations				
WT	D142A	E193A	E276A	W238A
90%	1%	~80%	~50%	~35%
% cells with green/red colocalization				

D

Plasmid cotransfected with GFP-UHRF1: DsRed-LIG1 with following mutations				
WT	R121E	T123D	R125A	R125E
90%	0%	0%	0%	1%
% cells with green/red colocalization				

Figure 3

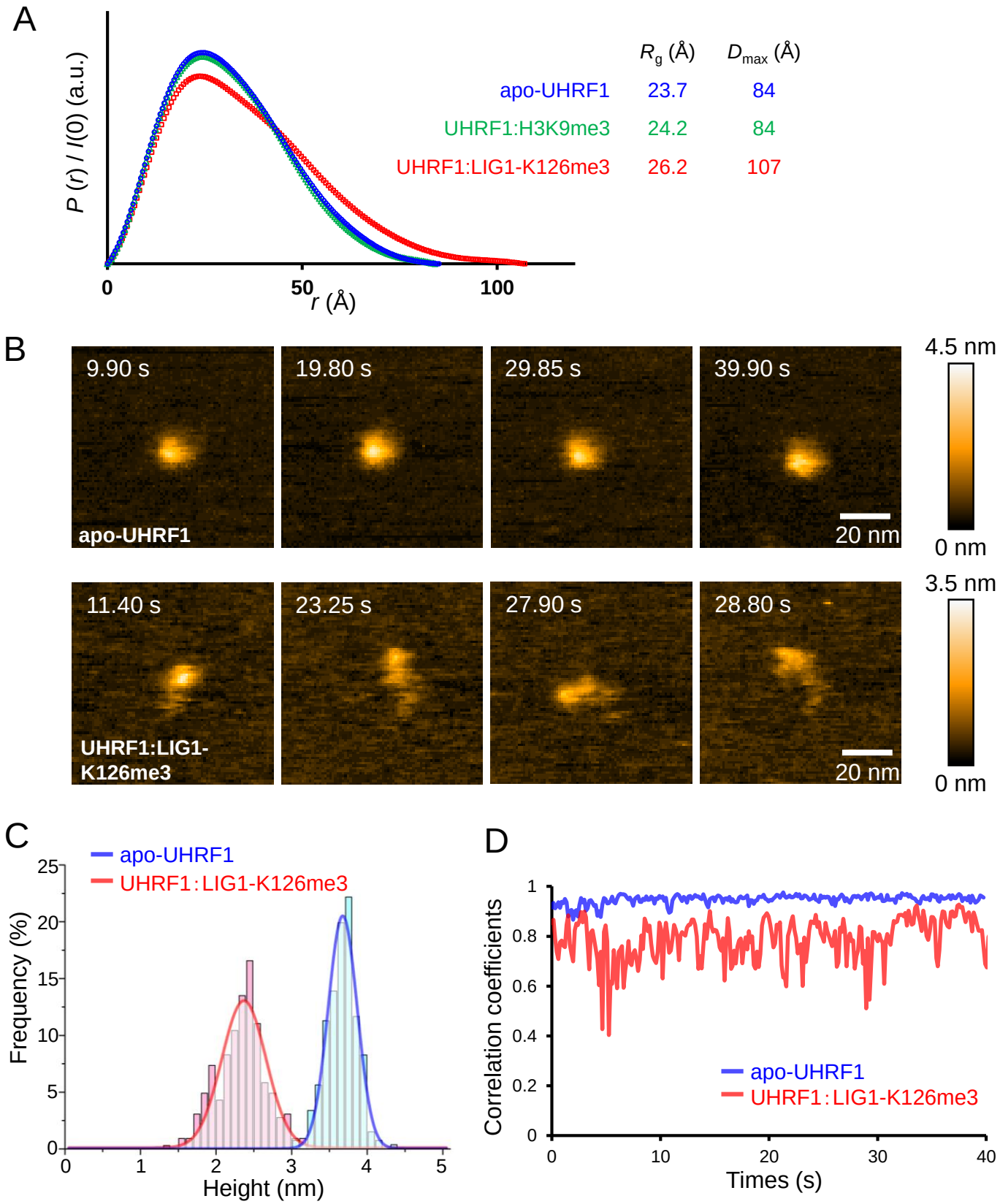
A
P (r) / I(0) (a.u.)
0
50
100
r (Å)
Rg (Å)
Dmax (Å)
apo-UHRF1
23.7
84
UHRF1:H3K9me3
24.2
84
UHRF1:LIG1-K126me3
26.2
107
B
9.90 s
19.80 s
29.85 s
39.90 s
apo-UHRF1
20 nm
4.5 nm
0 nm
11.40 s
23.25 s
27.90 s
28.80 s
UHRF1:LIG1-
K126me3
20 nm
3.5 nm
0 nm
C
apo-UHRF1
UHRF1:LIG1-K126me3
Frequency (%)
Height (nm)
D
Correlation coefficients
Times (s)
apo-UHRF1
UHRF1:LIG1-K126me3

Figure 4

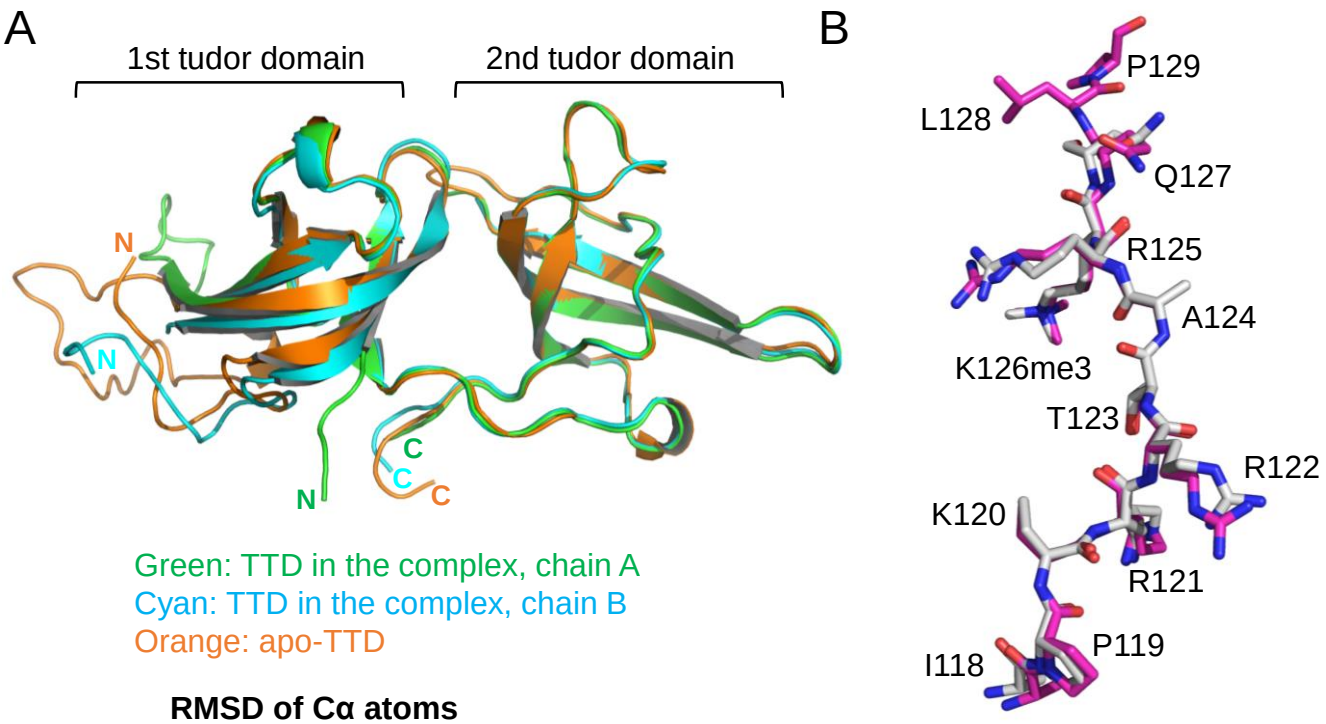

Green: TTD in the complex, chain A
Cyan: TTD in the complex, chain B
Orange: apo-TTD

RMSD of Cα atoms

apo-TTD: chain A	1.626 Å
apo-TTD: chain B	0.812 Å
chain A: chain B	1.401 Å

Magenta: LIG1 in complex, chain C
White: LIG1 in complex, chain D
RMSD of Cα atoms: 0.456 Å

Supplementary Figure S1 | Structural comparison of TTD and LIG1.
(A) Structures of apo-TTD and its complex with LIG1-K126me3 in the asymmetric unit are shown as orange, green and cyan cartoon model, respectively. The orientation is same as Figure 1A. (B) Stick-model structures of two LIG1 peptides in the asymmetric unit are colored magenta and white, respectively.

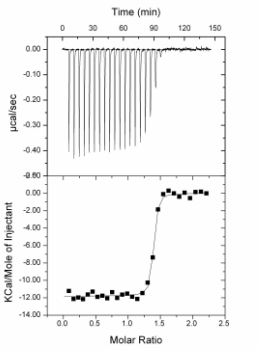

TTD wt :
LIG1-K126me3
K_D = 9.11 ± 3.80 nM

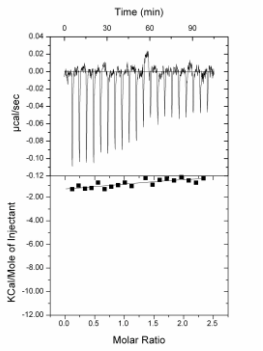

TTD D142A :
LIG1-K126me3
K_D = not detectable

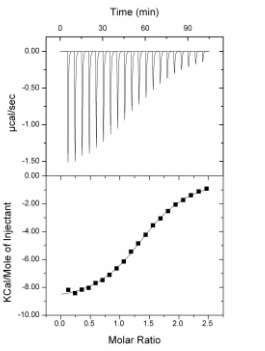

TTD Y188A/Y191A :
LIG1-K126me3
K_D = 5.38 ± 0.49 µM

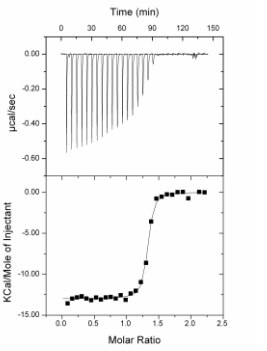

TTD E193A :
LIG1-K126me3
K_D = 23.0 ± 8.2 nM

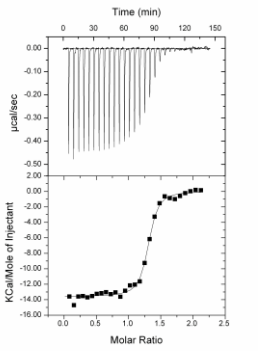

TTD E276A :
LIG1-K126me3
K_D = 49.7 ± 11.1 nM

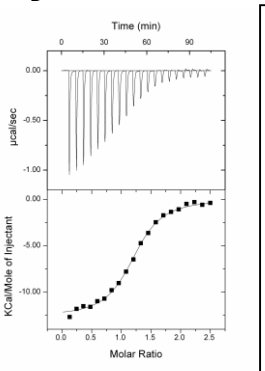

TTD W238A :
LIG1-K126me3
K_D = 1.06 ± 0.04 µM

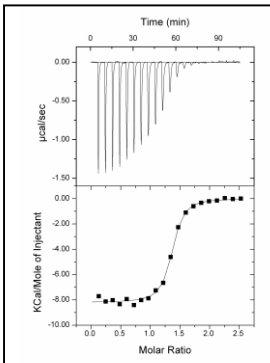

TTD wt :
LIG1-K126me0
K_D = 250 ± 35 nM

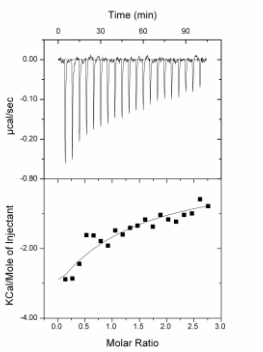

TTD wt : LIG1-
R121A/K126me3
K_D = >55 µM

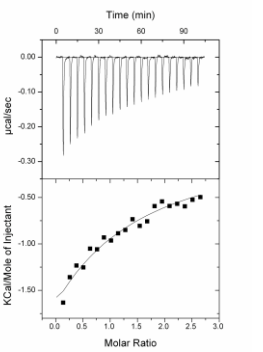

TTD wt : LIG1-
T123ph/K126me3
K_D = >104 µM

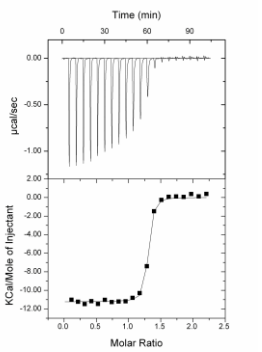

TTD wt : LIG1-
R125A/K126me3
K_D = 21.4 ± 1.1 nM

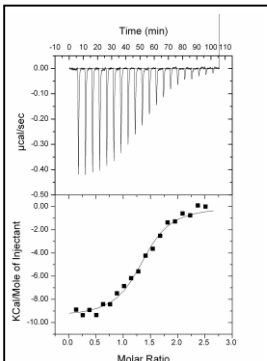

TTD wt :
$H3K9me3_{1-19}$
K_D = 612 ± 97 nM

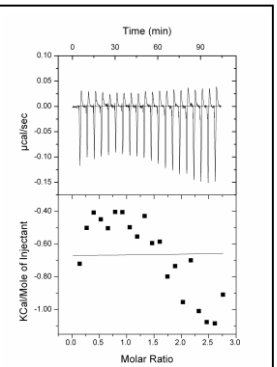

PHD wt :
LIG1-K126me3
K_D = not detectable

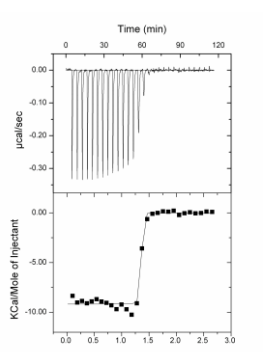

UHRF2 TTD wt :
LIG1-K126me3
K_D = < 0.43 nM

Supplementary Figure S2 | ITC thermograms (upper) and plots of corrected heat values (lower) for the binding of the LIG1 peptides to the TTD, PHD or UHRF2 TTD.

The first data point of each measurement was omitted from the plots in the lower panels and parameter fittings.

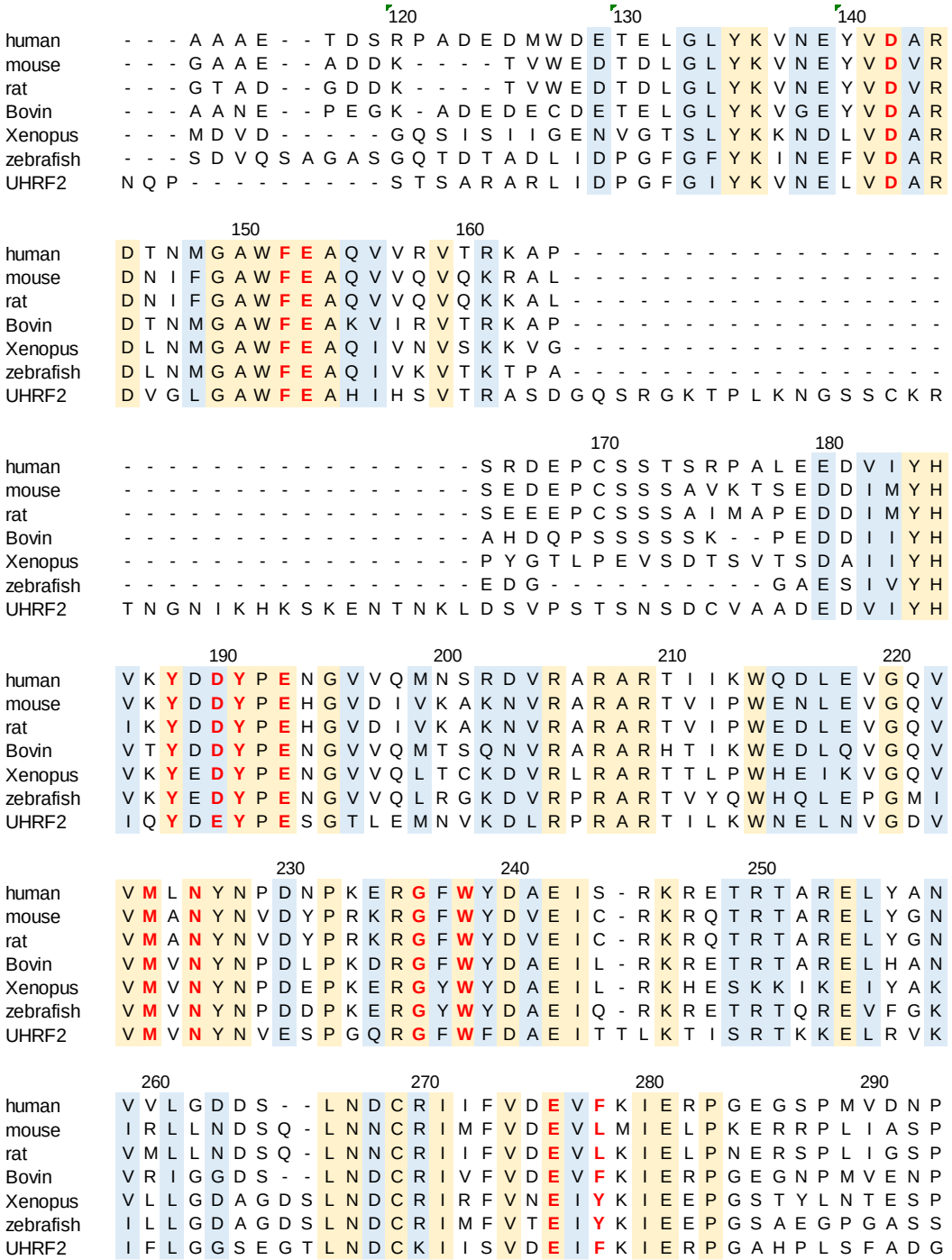

Supplementary Figure S3 | Multiple sequence alignment of the TTD region in UHRF1 proteins and human UHRF2. Numbering is based on the sequence of human UHRF1. Letters in red indicates the residues involved in recognition of LIG1. Fully and partially conserved amino acids are highlighted in light-orange and blue, respectively.

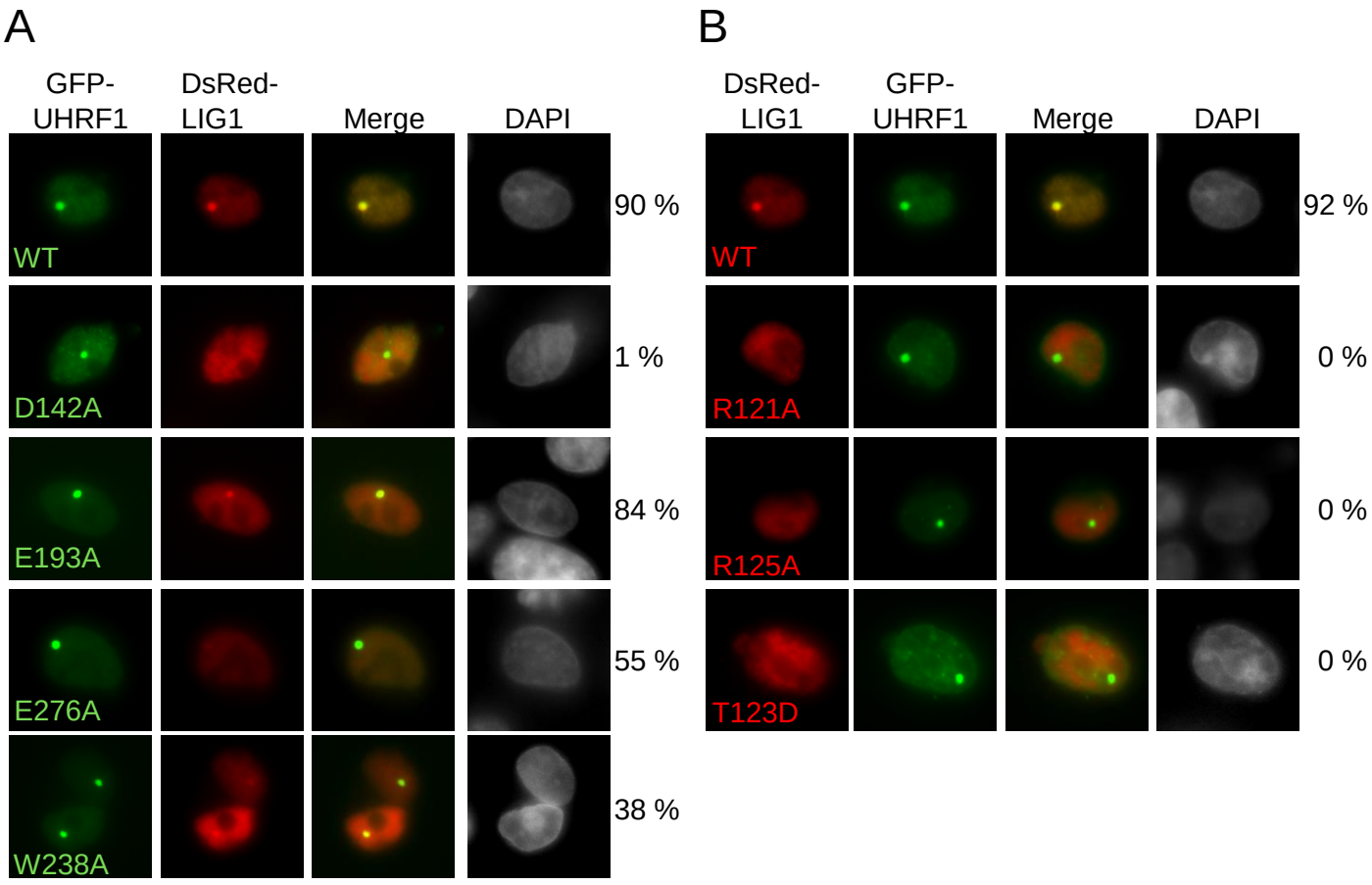

Supplementary Figure S4 | The F3H assay confirms the interaction between UHRF1 and LIG1 mutants. (A) Illustrative F3H images with UHRF1 point mutants. n = 100 cells scored in at least two independent experiments in this and all subsequent F3H data. (B) Illustrative F3H images with LIG1 point mutants.

A

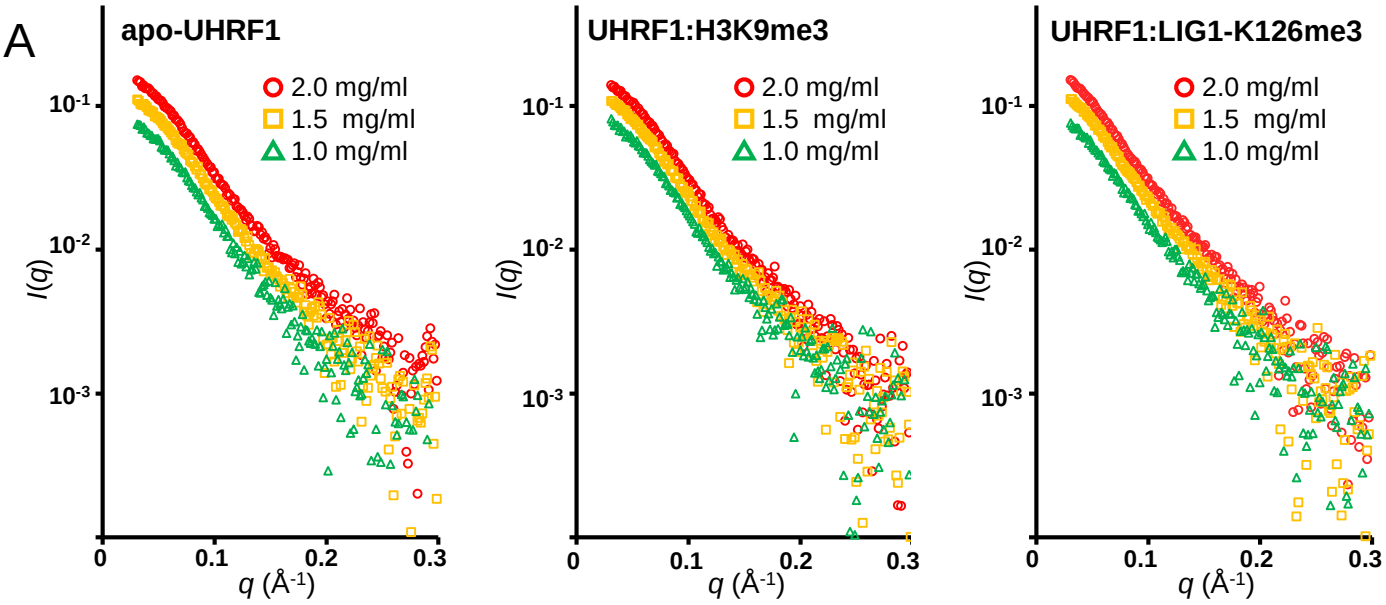

B

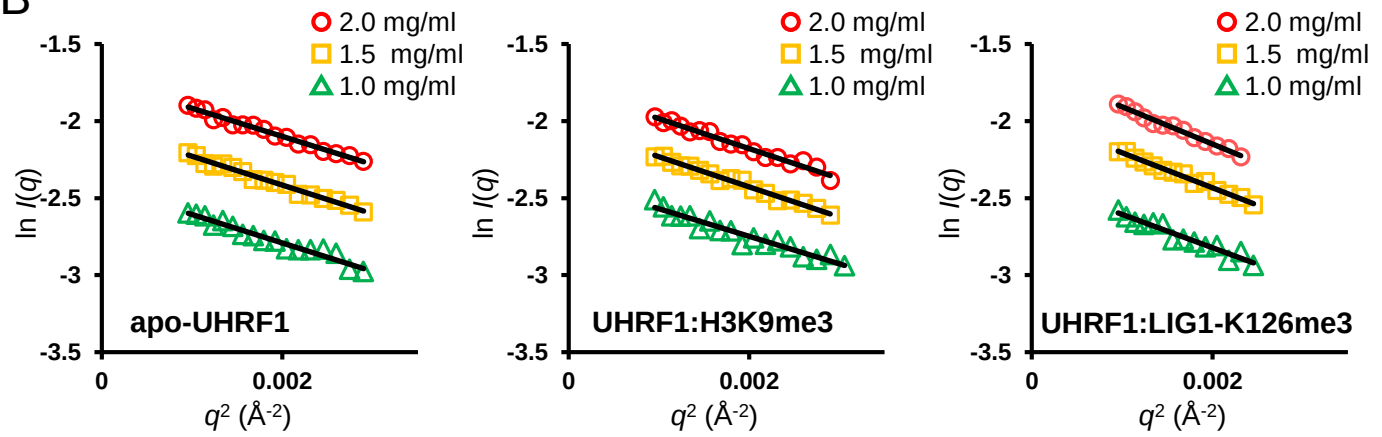

C

	Conc. (mg/ml)	R_g *a (Å)	R_g real *b (Å)	MW *c	theoretical MW
apo-TTD-PHD	2.0	23.5	24.6	27.5	28.3
	1.5	23.7		28.1	
	1.0	23.6		27.4	
TTD-PHD:H3K9me3	2.0	24.1	24.5	30.4	29.7
	1.5	24.2		30.1	
	1.0	23.2		32.4	
TTD-PHD:LIG1-K126me3	2.0	26.9	28.1	31.2	30.0
	1.5	26.2		30.1	
	1.0	25.4		29.6	

Supplementary Figure S5 | SAXS measurements of experimental *I*(*q*) profiles and Guinier plots of TTD-PHD with or without LIG1-K126me3 or H3K9me3 peptides.

(A) *I*(*q*) profiles of apo-TTD-PHD (left) and its complex with H3K9me3 (middle) and LIG1-K126me3 (right), obtained from SAXS data. The SAXS data of scattering curves were collected at three different protein concentrations, 2.0 (red), 1.5 (orange) and 1.0 mg/ml (green). (B) Guinier plots apo-TTD-PHD (left) and its complex with H3K9me3 (middle) and LIG1-K126me3 (right). (C) SAXS parameters for UHRF1 TTD-PHD and its complex with LIG1-K126me3 or H3K9me3. *a based on Guinier analysis. *b calculated from *P*(*r*) function. *c MW: molecular weight estimated from SAXS data of Lysozyme

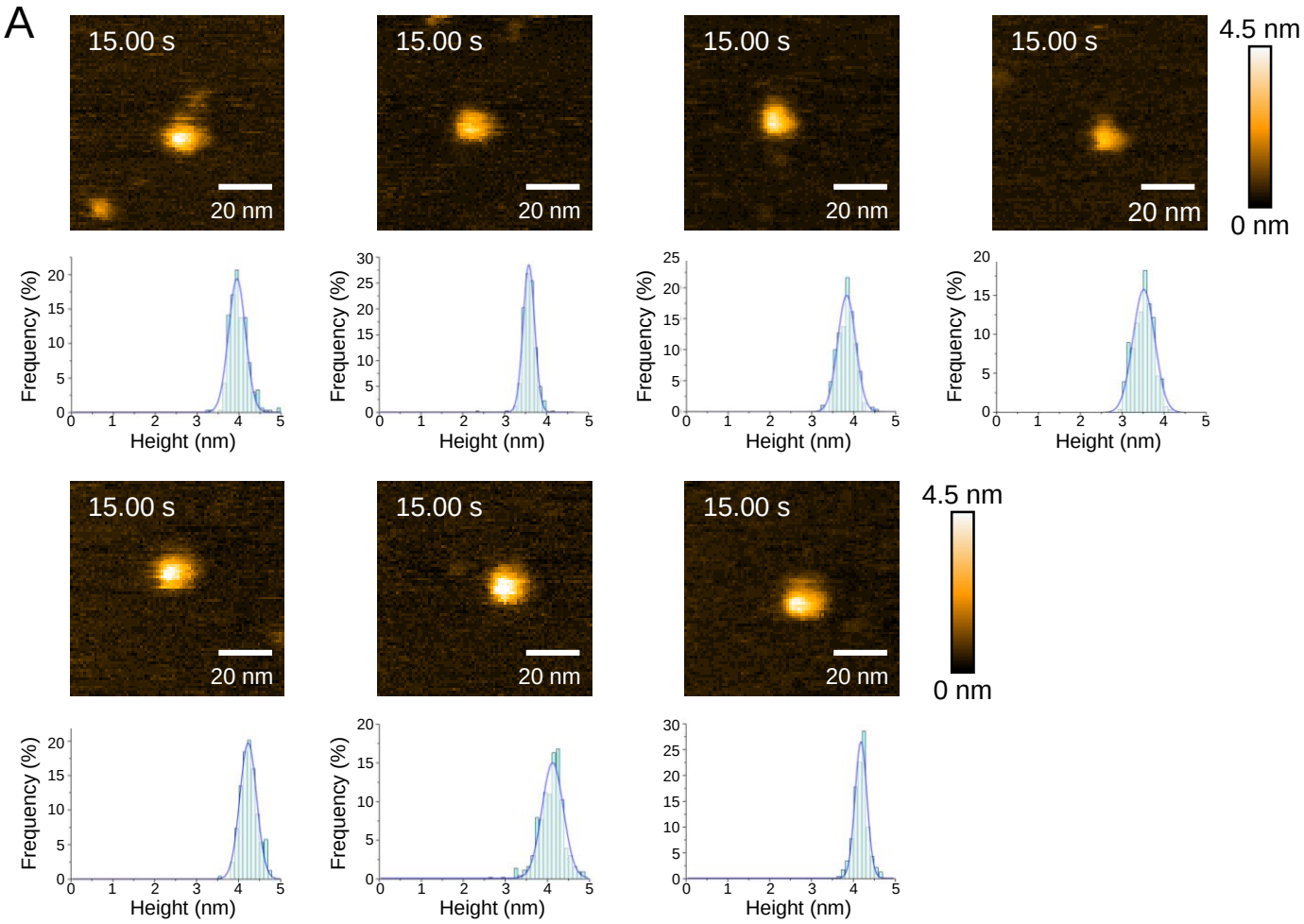

Supplementary Figure S6 | HS-AFM observations of apo-UHRF1
(A) AFM images and height analysis of seven representative molecules. Z-scale is 4.5 nm. (B) Time courses of 2D correlation coefficients between the sequential HS-AFM images of seven representative molecules.

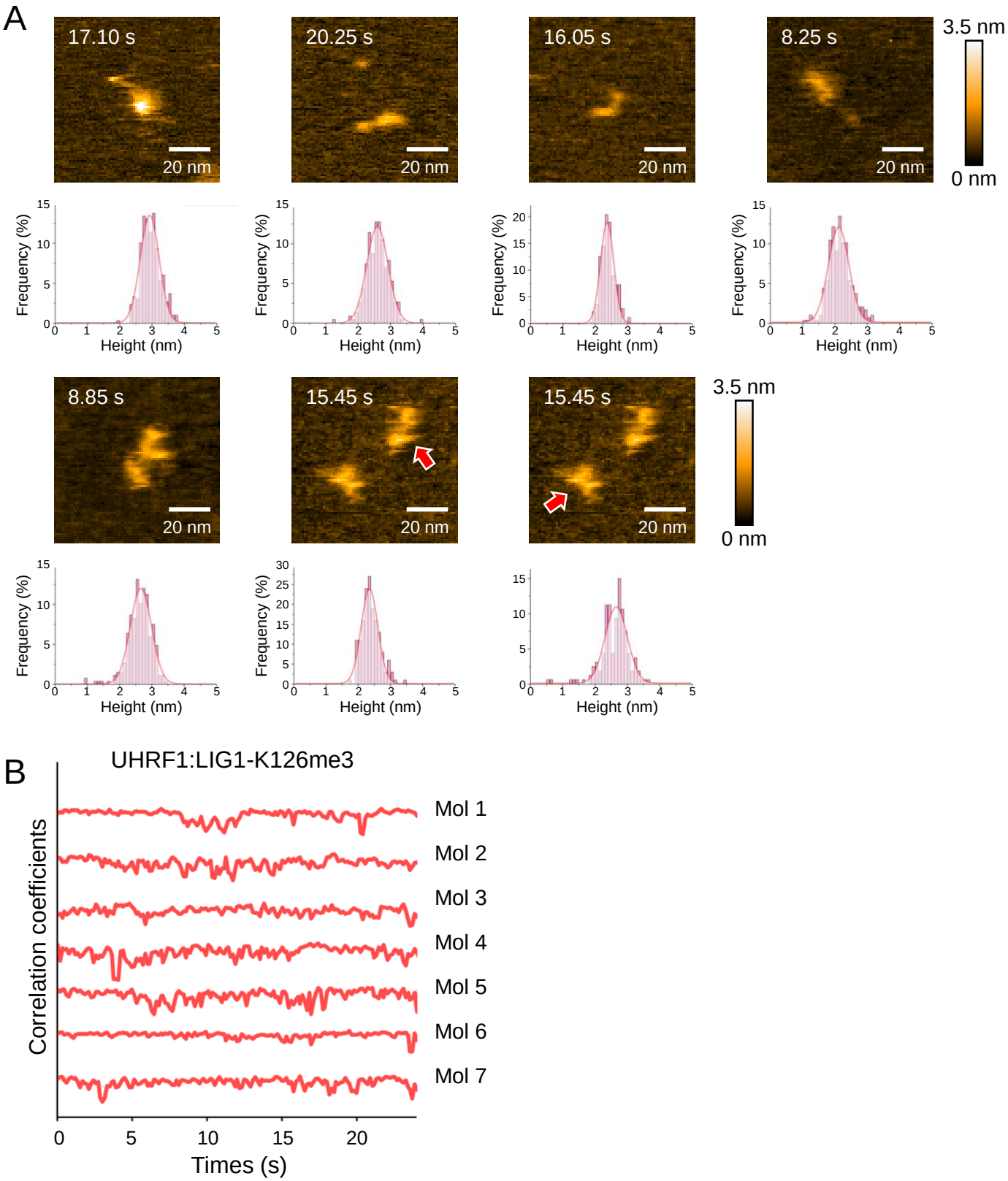

Supplementary Figure S7 | HS-AFM observations of UHRF1:LIG1-K126me3
(A) AFM images and height analysis of seven representative molecules. Z-scale is 3.5 nm.(B) Time courses of 2D correlation coefficients between the sequential HS-AFM images of seven representative molecules.